HHS Public Access

Author manuscript

Cell Rep. Author manuscript; available in PMC 2021 April 16.

Published in final edited form as:

Cell Rep. 2021 March 23; 34(12): 108892. doi:10.1016/j.celrep.2021.108892.

On the role of p53 in the cellular response to aneuploidy

Akshay Narkar[1,2,8], **Blake A. Johnson**[1,3,8], **Pandurang Bharne**[1], **Jin Zhu**[1], **Veena Padmanaban**[1], **Debojyoti Biswas**[4], **Andrew Fraser**[1], **Pablo A. Iglesias**[1,4,5], **Andrew J. Ewald**[1], **Rong Li**[1,6,7,9,*]

[1]Center for Cell Dynamics and Department of Cell Biology, Johns Hopkins University, School of Medicine, Baltimore, MD 21205, USA

[2]McKusick-Nathans Institute of Genetic Medicine, Johns Hopkins University School of Medicine, Baltimore, MD 21205, USA

[3]Medical Scientist Training Program, Johns Hopkins University School of Medicine, Baltimore, MD 21205, USA

[4]Electrical and Computer Engineering, Whiting School of Engineering, Johns Hopkins University, Baltimore, MD 21218, USA

[5]Department of Biomedical Engineering, Johns Hopkins University, Baltimore, MD 21218, USA

[6]Department of Chemical and Biomolecular Engineering, Whiting School of Engineering, Johns Hopkins University, Baltimore, MD 21205, USA

[7]Mechanobiology Institute and Department of Biological Sciences, National University of Singapore, Singapore 117411, Singapore

[8]These authors contributed equally

[9]Lead contact

SUMMARY

Most solid tumors are aneuploid, and p53 has been implicated as the guardian of the euploid genome. Previous experiments using human cell lines showed that aneuploidy induction leads to p53 accumulation and p21-mediated G1 cell cycle arrest. We find that adherent 2-dimensional (2D) cultures of human immortalized or cancer cell lines activate p53 upon aneuploidy induction, whereas suspension cultures of a human lymphoid cell line undergo a p53-independent cell cycle arrest. Surprisingly, 3D human and mouse organotypic cultures from neural, intestinal, or mammary epithelial tissues do not activate p53 or arrest in G1 following aneuploidy induction. p53-deficient colon organoids have increased aneuploidy and frequent lagging chromosomes and

*Correspondence: rong@jhu.edu.

AUTHOR CONTRIBUTIONS

Conceptualization, A.N. and R.L.; investigation, A.N., B.A.J., P.B., J.Z., V.P., A.F., A.J.E., and R.L.; analysis, A.N., B.A.J., P.B., and D.B.; writing, A.N., B.A.J., J.Z., and R.L. All authors discussed the results and commented on the manuscript.

SUPPLEMENTAL INFORMATION

Supplemental Information can be found online at https://doi.org/10.1016/j.celrep.2021.108892.

DECLARATION OF INTERESTS

The authors declare no competing interests.

multipolar spindles during mitosis. These data suggest that p53 may not act as a universal surveillance factor restricting the proliferation of aneuploid cells but instead helps directly or indirectly ensure faithful chromosome transmission likely by preventing polyploidization and influencing spindle mechanics.

Graphical Abstract

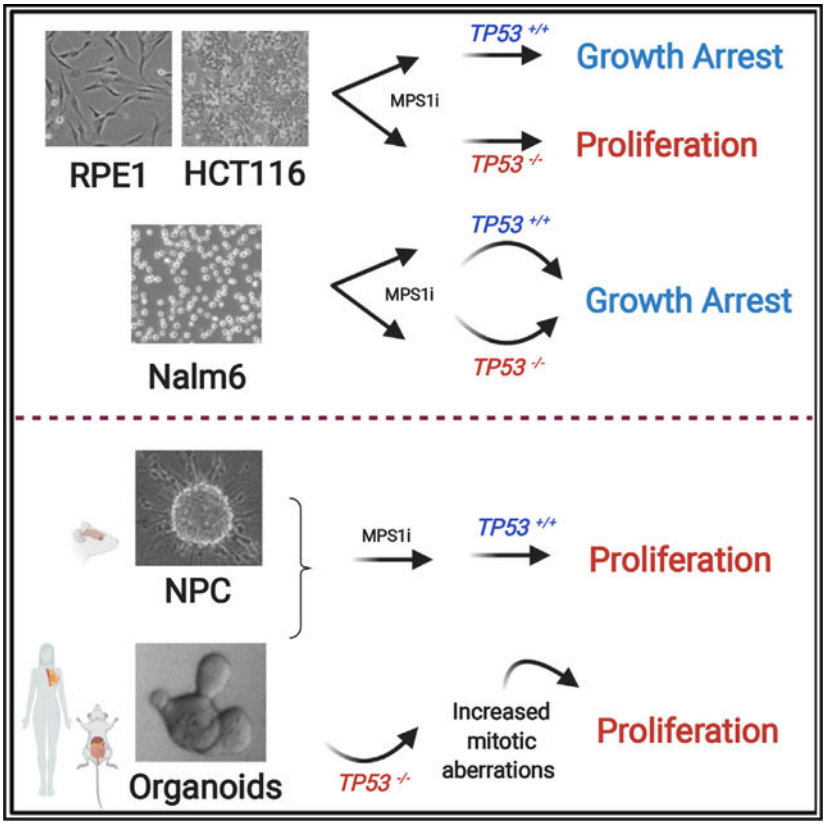

In brief

By investigating how various cell lines and organotypic cultures respond to the induction of aneuploidy, Narkar et al. show that p53 does not constitute a universal surveillance mechanism against aneuploidy. p53 prevents aneuploidy by limiting mitotic errors in colon organoids.

INTRODUCTION

Aneuploidy refers to the state of unequal chromosome copy numbers and is one of the most prominent genomic aberrations in solid tumors (Beroukhim et al., 2010; Lengauer et al., 1998; Taylor et al., 2018; Weaver and Cleveland, 2006; Zack et al., 2013). In unicellular eukaryotes, it was shown that aneuploidy, by altering the stoichiometry of a large number of genes, can result in dramatic changes in cellular phenotypes and physiology and confer evolutionary adaptation under selective pressure (Dephoure et al., 2014; Kaya et al., 2015; Pavelka et al., 2010; Selmecki et al., 2006; Sterkers et al., 2012; Sunshine et al., 2015; Torres et al., 2007; Yona et al., 2012). Such basic insight about aneuploidy helps explain recent

findings that karyotype alterations are associated with cancer initiation as well as the emergence of drug resistance (Cai et al., 2016; Davoli et al., 2013; Graham et al., 2017; Lane et al., 2014; Lee et al., 2011; Navin et al., 2011; Sack et al., 2018; Stichel et al., 2018; Yang et al., 2019). Indeed, cancer may be viewed as a disease of cellular evolution in a multicellular setting, whereby cells of metazoans turn to resembling unicellular organisms that are free to undergo evolutionary adaptation for better survival and proliferation through gross genomic alterations (Chen et al., 2015; Duesberg et al., 2001; Gerstung et al., 2020; Nowell, 1976).

It is thought that a key difference between mammals and freely adapting unicellular eukaryotes is the presence of p53 that guards genome stability by regulating the DNA damage response, senescence, and apoptosis. (Aylon and Oren, 2011; Hafner et al., 2019; Kastenhuber and Lowe, 2017; Mello and Attardi, 2018; Mijit et al., 2020; Reinhardt and Schumacher, 2014). The loss of functional p53 has been associated with the onset of many metastatic cancers with heightened chromosomal instability; in contrast, an increased p53 gene copy number is thought to be chemopreventive (Bykov et al., 2018; Donehower et al., 2019; Sulak et al., 2016; Wasylishen and Lozano, 2016). Studies in recent years have further suggested roles for p53 in limiting the proliferation of aneuploid cells. However, these studies were limited to established human cell lines that were chromosomally stable and near diploid, such as RPE1, an hTERT-immortalized retinal pigmented epithelial cell line; HCT116, a colon carcinoma cell line; and a few other cell lines (Cianchi et al., 1999; Giam et al., 2019; Hinchcliffe et al., 2016; Janssen et al., 2011; Kurinna et al., 2013; Li et al., 2010; Potapova et al., 2016; Santaguida et al., 2017; Soto et al., 2017; Thompson and Compton, 2010). Recent studies also revealed complex interplay between p53 and several other genome-protective proteins, such as p38, H3.3, and BCL9L (Hinchcliffe et al., 2016; López-García et al., 2017; Simões-Sousa et al., 2018). However, it has been unclear whether a universal signal elicited by abnormal karyotypes may be sensed by the p53 pathway or whether karyotype-specific stress states are sensed through diverse mechanisms and converge upon p53 activation. It was also unknown whether cell type or growth environment could contribute to the p53-mediated response to aneuploidy.

Here, we investigated p53 regulation and downstream cell fate after aneuploidy induction in diverse cell culture models. We set out to answer the following three questions. (1) Is the relationship between aneuploidy induction and p53 activation universal? (2) What are the downstream cell fate consequences after acute aneuploidy induction in different types of cell culture models? (3) Does p53 play a direct or indirect role in faithful mitosis rather than sensing aneuploid cells after erroneous mitosis? Although we confirm that upon acute aneuploidy induction by treating cells with an inhibitor of the spindle assembly checkpoint (SAC) kinase MPS1 (MPS1i), p53 and p21 were upregulated and cause growth arrest in RPE1 and HCT116 cell lines, this response was not conserved in three-dimensional (3D) organotypic cultures of primary cells from mouse and human tissues. Live imaging in colon organoids further supports a role for p53 in mitotic fidelity, as opposed to limiting the proliferation of aneuploid cells.

RESULTS

Induction of aneuploidy with MPS1i in mammalian cell lines and 3D organotypic cultures

To investigate the response to aneuploidy in a broadly representative panel of cell models, we included not only the previously used RPE1 and HCT116 cell lines but also Nalm6, a chromosomally stable pre-B cell lymphoma line that grows in suspension (Hurwitz et al., 1979), and 3D organotypic cultures of primary cells. Potentially influential parameters also included different stages of development, for which we included embryonic and adult mouse neural progenitor cells (eNPCs and aNPCs, respectively). For 3D cultures of primary cells that better mimic *in vivo* tissues, we also included human mammary organoids (hMOs) (Cheung et al., 2013) and mouse colon organoids (mCOs) (Sato and Clevers, 2013). To induce aneuploidy, each type of culture was treated with the MPS1 inhibitor NMS-P715 (Colombo et al., 2010) for 24 h followed by drug washout and recovery growth for 24 or 48 h in drug-free media to alleviate any direct drug effects before various analyses (Figure 1A). We first quantified the percent numerical aneuploidy by chromosome counting of metaphase spreads 24 h after the MPS1i treatment. For RPE1, HCT116, Nalm6, hMOs, and mCOs, the basal whole-chromosome aneuploidy levels were low in untreated cultures, and a significant increase in aneuploidy percentages, to 45%–55%, was observed in each MPS1i-treated culture (Figure 1B). NPCs also showed increased aneuploidy after MPS1i treatment, but the basal aneuploidy percentages were higher, consistent with earlier reports (Rehen et al., 2005; Yang et al., 2003). The chromosome number distributions showed both gains and losses of chromosomes across most cell models, consistent with the production of aneuploidy as a result of random mitotic errors (Figures 1C and 1D). We also measured the doubling time for RPE1, HCT116, and mCOs and found it to be in the range of 16–22 h (Figure S1A). For metaphase spreads, Colcemid was used to arrest cells in metaphase. However, this limited our analysis to only cells that were able to enter mitosis, which could result in an underestimation of the true aneuploidy frequency. To also analyze interphase cells, we performed chromosome counting in RPE1, HCT116, and mCOs by using Calyculin A, which causes premature chromosome condensation and does not require mitotic entry. We observed close to 60% aneuploidy in RPE1, HCT116, and mCOs after MPS1i treatment using this method (Figure 1E). We also performed live-cell imaging of H2B-mNeon RPE1, HCT116, and mCOs and observed comparable increases in lagging chromosome frequency during MPS1i treatment. (Figure 1F). Together, these analyses demonstrate that we induced similar levels of aneuploidy in each cellular system. Importantly, our method of inducing aneuploidy did not involve cell synchronization, as some agents altering cell cycle progression may cause DNA damage (Darzynkiewicz et al., 2011; Halicka et al., 2016), which could activate p53. As expected, pH2AX immunoblots and immunofluorescence staining showed that the MPS1i treatments used in our experiments did not induce DNA damage (Figures S1B–S1D). We also quantified the frequency of micronuclei—a possible source of DNA damage following MPS1i-induced chromosome missegregation (Crasta et al., 2012; Terradas et al., 2009; Zhang et al., 2015). Micronuclei formed infrequently and at a similar frequency in MPS1i-treated RPE1, HCT116, and mCOs (Figure S1E), suggesting that micronuclei formation was not a source of DNA damage in our study.

Adherent RPE1 and HCT116 but not suspension Nalm6 cells depend on p53 for growth arrest after aneuploidy induction

We next determined the effect of acute aneuploidy induction on p53 and the CDK inhibitor CDKN1A (p21), a well-studied direct transcriptional target of p53 that controls cell cycle progression (Dulić et al., 1994; el-Deiry et al., 1993). p53 is known to be regulated predominantly by posttranslational modifications that affect its stability or nuclear accumulation (Haupt et al., 1997; Kruse and Gu, 2009; Oren, 1999). Acute induction of aneuploidy using drugs that perturb mitosis or SAC led to increased p53 stabilization and a consequent G1 arrest upon transcriptional activation of p21 (Kollu et al., 2015; Li et al., 2010). We observed significant increases in p53 levels in the adherent RPE1 and HCT116 cells and suspension Nalm6 cells, but not in the NPCs or 3D organotypic cultures (presented further below), after aneuploidy induction using MPS1i (Figures 2A and 2B). Additionally, nuclear localization of p53 was confirmed in HCT116 and RPE1 cells by immunofluorescence staining (Figures S1F and S1G). All cell lines showed increased p53 protein abundance upon treatment with nutlin-3 (Shen and Maki, 2011), which stabilizes p53 by disrupting the p53-MDM2 complex, and DNA damaging agents such as doxorubicin and bleomycin (Figures 2A, 3A, 3B, S1F, and S1G).

p53 plays a critical role in controlling cell proliferation and death in response to stress (Kastenhuber and Lowe, 2017; McKinley and Cheeseman, 2017). We examined whether p53 induction was associated with either cell cycle arrest or apoptosis by assaying DNA synthesis using the 5-ethynyl-2′-deoxyuridine (EdU) incorporation assay (Salic and Mitchison, 2008) and apoptosis using Annexin V and propidium iodide. In MPS1i-treated RPE1, HCT116, and Nalm6 cells, there was a significant reduction in EdU-positive cells (Figures 2C and 2D), consistent with a suppression of proliferation, but these populations did not display a significant increase in apoptotic cells (Figure S2E). Cell cycle analysis for RPE1, HCT116, and Nalm6 cells showed significant G1 arrest after aneuploidy induction (Figures S3A and S3B). To test the requirement for p53 in mediating this arrest, we used *TP53*$^{-/-}$ HCT116 (Bunz et al., 2002), RPE1 *TP53*$^{-/-}$ (Lambrus et al., 2016), and *TP53*$^{-/-}$ Nalm6 cells generated using CRISPR-Cas9. p53 knockout was confirmed in RPE1, HCT116, and Nalm6 cell lines by immunoblotting (Figure S2A). These lines lacking p53 did not show p21 upregulation after aneuploidy induction. Additional genotyping validation was performed for Nalm6 (Figure S2B). Deviation from the diploid chromosome number in these cells lacking p53 was observed even without MPS1i treatment (Figure S2C). p53 knockout rescued cell proliferation, as indicated by the increased EdU-positive cells, in MPS1i-treated HCT116 and RPE1 populations (Figures 2C and 2D). However, this rescue was not observed in Nalm6 *TP53*$^{-/-}$ suspension cells (Figure 2D), suggesting that, although p53 was induced after aneuploidy, it was not required for the reduced proliferation in Nalm6 cells. *TP53*$^{-/-}$ Nalm6, but not HCT116 or RPE1, cells also showed an increase in apoptosis after aneuploidy induction (Figure S2E).

3D organotypic cultures do not activate p53 or undergo growth arrest in response to aneuploidy

The three established cell lines (RPE1, HCT116, and Nalm6) responded to aneuploidy as expected despite a lack of p53 dependence for the growth arrest in Nalm6 cells, whereas we

did not observe an increase in p53 or p21 protein abundance after aneuploidy induction in 3D cultures of NPCs, mCOs, or hMOs (Figures 2B, 3A, and 3B). As a positive control, treatment with nutlin, doxorubicin, or bleomycin increased p53 and p21 protein abundance, suggesting that p53 is generally functional in these cell models. Consistent with a lack of p53 activation in 3D organotypic cultures after aneuploidy induction, an EdU incorporation assay showed unimpeded cell proliferation, in contrast to reduced proliferation of the same cultures treated with nutlin or DNA-damaging agents (Figures 3C, 3D, and S2D). Also, cell cycle analysis for mCOs did not show significant G1 arrest after aneuploidy (Figure S3B). A recent study demonstrated that cellular architecture has profound impacts on chromosome segregation fidelity (Knouse et al., 2018). To rule out the possibility that the differential responses to aneuploidy observed between the adherent epithelial cell lines and organotypic cultures was due to a 2D versus 3D culture environment, we cultured HCT116 cells as 3D spheres in Matrigel (Figure S4A). These cells grew into spherical structures with high-level EdU incorporation, indicating active proliferation (Figure S4C). Upon aneuploidy induction, HCT116 cells cultured in 3D exhibited similar levels of p53 and p21 increase and growth arrest, as observed for those cultured in 2D (Figures S4B, S4C, and S4D). This result suggests that the difference in aneuploidy responses observed among the different cell types tested was unlikely attributed to 2D versus 3D culture environment.

Trp53$^{-/-}$ mCOs exhibit frequent mitotic aberrations

Although mCOs did not exhibit elevated p53 or G1 arrest after aneuploidy induction, mCOs generated from *Trp53*$^{-/-}$ mice showed around 40% aneuploidy (Figures S5A and S5B) compared to (Figure 1B) 15% aneuploidy in *Trp53*$^{+/+}$ mCOs, suggesting that p53 may have a role in preventing aneuploidy occurrence instead of inhibiting the proliferation of aneuploid cells. To test this, *Trp53*$^{+/+}$ and *Trp53*$^{-/-}$ mCOs were transduced with H2B-mNeon, and mitotic cell divisions were observed using live 3D confocal imaging (Videos S1 and S2). Mitotic aberrations including multipolar divisions and lagging chromosomes were quantified from the live movies. The fraction of cells exhibiting lagging chromosomes was increased in *Trp53*$^{-/-}$ when compared to *Trp53*$^{+/+}$ mCOs, and there was also an increase in multipolar divisions (Figures 4A and 4B; Videos S3 and S4). In the presence of low-dose nocodazole, the time in mitosis (from nuclear envelope breakdown [NEBD] to anaphase onset) was lengthened significantly in both *Trp53*$^{+/+}$ and *Trp53*$^{-/-}$ mCOs, suggesting that p53 loss did not disrupt canonical kinetochore-based SAC signaling (Figure 4C). Interestingly, induction of SAC by low-dose nocodazole reduced the frequency of lagging chromosomes in *Trp53*$^{-/-}$ mCOs, suggesting that lengthening mitotic duration facilitates error correction in the p53-deficient background. The lagging chromosomes could occur secondary to polyploidization or centrosome amplification (Fukasawa et al., 1996; Galipeau et al., 1996; Lopes et al., 2018). Analysis of nuclear volume immediately before (G2) and after (G1) mitosis from the videos confirmed nuclear volume scales with DNA content (Figure 4D). The G2 nuclear volume of cells with lagging chromosomes in bipolar spindles was not significantly different from cells undergoing normal mitoses (Figure 4D). In contrast, the average G2 nuclear volume of cells that underwent multipolar divisions was approximately double that of cells with normal divisions (Figure 4D). This finding suggests that tetraploidization occurred prior to multipolar divisions but was not the cause of lagging chromosomes in *Trp53*$^{-/-}$ cells with bipolar mitoses. Centrosome amplification, independent

of genome doubling, gives rise to lagging chromosomes (Ganem et al., 2009). In *Trp53*$^{-/-}$ mCOs, increased centrosome number determined by pericentrin immunofluorescence was exclusively associated with increased mitotic chromatin volume (Figure 4E). Total pericentrin fluorescence intensity per centrosome was similar in cells with two centrosomes and those with more than two centrosomes in *Trp53*$^{+/+}$ and *Trp53*$^{-/-}$ mCOs (Figure S5C), indicating centrosome clustering was not impeding our ability to accurately count centrosome number. This result suggests that extra centrosomes are associated with tetraploidization in *Trp53*$^{-/-}$ mCOs. Therefore, centrosome amplification is unlikely to be the cause of lagging chromosomes in diploid *Trp53*$^{-/-}$ cells in mCOs.

DISCUSSION

We have examined the generality of p53 upregulation and cellular responses after acute induction of aneuploidy in a variety of cell models linked to different tissue origins and growth environments. Based on earlier findings in immortalized and cancer cell lines such as RPE1 and HCT116, our original interest was to identify aneuploidy-associated signals that induce p53 activation in these cells. However, our inability to generate a similar response in NPCs and the observation of a p53-independent response in Nalm6 pre-B lymphocytes suggested to us that p53 activation after aneuploidy induction is not necessarily a universal response but may be more cell line specific. This led us to conduct a more comprehensive investigation of cellular responses in 3D organoid cultures. We found that induction of aneuploidy does not result in p53 accumulation or cell proliferation arrest in organotypic cultures from epithelial tissues of neural, intestinal, and mammary origins from mouse or human. The p53 response and cell cycle fate after aneuploidy induction in each of the cellular systems used in our study are summarized in Table S1. Testing organoids derived from a broader range of tissues will allow further assessment of the generality of our findings.

We recognized that two previous studies found that not all aneuploid RPE1 cells resulting from erroneous mitoses activate p53 (Santaguida et al., 2017; Soto et al., 2017). Those studies concluded that the p53-mediated G1 arrest may be more associated with complex aneuploidy or structural aneuploidy in RPE1 cells. Our data in RPE1 and HCT116 cells do not contradict these conclusions but differ in the degree of p53 induction. Also, our data do not address the nature of the signal that activates p53. In our experiments, the 24-h MPS1i treatment did not induce DNA damage, although we cannot rule out that continued propagation of aneuploid cells in organotypic cultures could lead to DNA damage and p53 activation at a later time. Responses to aneuploidy induction in the *Drosophila* brain varied in different cell types and at different times (Mirkovic et al., 2019). The different p53 response observed in our study was also unlikely to be due strictly to a 2D versus 3D culturing system because 3D cultures of HCT116 cells showed a similar p53 response to those cultured in 2D.

Given that 3D organotypic cultures of primary cells are better mimics of native tissues than immortalized or cancer cell lines (Schutgens and Clevers, 2020), our findings do not support the notion that p53 acts in a surveillance mechanism against aneuploidy *in vivo*. It is possible that stress associated with artificially immortalized or cancer cell lines passaged in

the conventional cell culture environment combined with the stress caused by aneuploidy can trigger p53 accumulation and cell cycle arrest. Interestingly, the Nalm6 pre-B lymphocyte cell line showed a p53-independent cell cycle arrest following aneuploidy induction, suggesting that another yet unidentified mechanism exists to limit the proliferation of aneuploid blood cells. This may be in line with the observation that certain hematological cancers show lower *TP53* mutational rates (Olivier et al., 2010; Prokocimer et al., 2017; Robles et al., 2016). Further studies are warranted to understand the specific molecular mechanisms driving the differences in p53 response to aneuploidy induction.

Although our data do not support a role for p53 in aneuploidy surveillance in organotypic cultures, there is strong evidence indicating that the loss of p53 is associated with chromosome instability and poor prognosis in the development of several cancers (Donehower et al., 2019; Foijer et al., 2014; Fujiwara et al., 2005; Watson and Elledge, 2017), and a majority of tumors show varied *TP53* mutations (Clausen et al., 1998; Muller and Vousden, 2013). Live-cell imaging of $Trp53^{+/+}$ and $Trp53^{-/-}$ mCOs showed that mitotic errors, including lagging chromosomes and multipolar mitoses, occurred frequently in cells lacking p53, consistent with several published studies (Artegiani et al., 2020; Drost et al., 2015). Our analysis also indicates that tetraploidization is likely to be a precursor to multipolar divisions in $Trp53^{-/-}$ mCOs. There has been significant debate surrounding the role of p53 in suppressing the division of tetraploid cells (Andreassen et al., 2001; Ganem and Pellman, 2007; Horii et al., 2015; Uetake and Sluder, 2004; Wong and Stearns, 2005). Recent work showed that p53 transcriptionally regulates multiple genes important for mitotic processes, including *Aurka*, *Foxm1*, and *Plk4*, and that a loss of p53 leads to polyploidization during liver regeneration *in vivo* (Kurinna et al., 2013). Aberrant expression of these mitotic genes in the absence of p53 may drive tetraploidization and lead to multipolar divisions in $Trp53^{-/-}$ mCOs. Importantly, tetraploidization was found to be sufficient to drive tumorigenesis in cells lacking p53 (Fujiwara et al., 2005).

The underlying cause of the observed lagging chromosomes in $Trp53^{-/-}$ mCOs remains unclear. An increase in lagging chromosomes was also reported for p53-deficient human liver and colon organoids (Artegiani et al., 2020; Drost et al., 2015). Our results suggest that lagging chromosomes in bipolar divisions do not occur secondarily to polyploidization or centrosome amplification. p53 loss does not appear to disrupt SAC activation induced by nocodazole treatment, and in fact, SAC activation reduced the occurrence of lagging chromosomes. It is thus possible that the loss of p53 directly or indirectly leads to the type of mitotic problems, such as faulty kinetochore-microtubule attachments, that can be corrected when mitosis is lengthened by SAC. Interestingly, lagging chromosomes can impede cytokinesis and result in the generation of tetraploid cells (Lens and Medema, 2019; Shi and King, 2005; Steigemann et al., 2009). Thus, it is possible that lagging chromosomes in $Trp53^{-/-}$ mCOs contribute to the generation of tetraploid cells that then undergo multipolar divisions. A better understanding of the precise role for p53 in suppressing aneuploidy in physiological settings may allow for the development of therapeutics for the prevention of mitotic abnormalities and, ultimately, cancers associated with p53 loss.

STAR★METHODS

RESOURCE AVAILABILITY

Lead contact—Further information and requests for resources and reagents should be directed to and will be fulfilled by the Lead Contact, Rong Li (rong@jhu.edu).

Materials availability—This study did not generate new unique reagents.

Data and code availability—The published article includes all datasets and code generated or analyzed during this study.

EXPERIMENTAL MODEL AND SUBJECT DETAILS

Animals—Wild-type C57BL/6J were purchased from the Jackson Laboratory and *Trp53*$^{-/-}$ mice (The Jackson Laboratory) were a gift from Andrew Holland's lab. Mice used for NPC and colon organoid isolation were between 6 and 12 weeks old. Male and female wild-type mice were used for NPC and colon organoid isolation and male *Trp53*$^{-/-}$ mice were used for colonoid isolation. All mouse care and use were approved by the Institutional Animal Care and Use Committee at the Johns Hopkins University.

Tissues—Normal mammary reduction samples were acquired from the Cooperative Human Tissue Network in compliance with a study protocol (NA_00077976) that was categorized as exempt/not human subject research by the Johns Hopkins School of Medicine Institutional Review Board. Each sample was deidentified prior to receipt and shipped overnight in basal DMEM/RPMI medium.

Cell culture—hTERT-RPE1 were grown at 37°C in 5% CO2 in DMEM supplemented with 10% fetal bovine serum (FBS). RPE-1 *TP53*$^{-/-}$ cells were a gift from Andrew Holland's lab. HCT116 cells were grown at 37°C in 5% CO2 in McCoy's media supplemented with 10% fetal bovine serum (FBS). HCT116 *TP53*$^{-/-}$ cells were a gift from Bert Vogelstein lab. Nalm6 cells were a gift from Mike Tyers' lab and were grown at 37°C in 5% CO2 in RPMI supplemented with 10% fetal bovine serum (FBS). Nalm6 *TP53*$^{-/-}$ cells were generated in-house using lentiCRISPRV2. *TP53* knockout was confirmed by sequencing and western blot validation. Neuronal Progenitor cells isolated from embryonic mouse brain (frontal) and adult 10-week-old mice SVZ and DG areas and cultured as neurospheres on ultra-low attachment plates using DMEM and Ham's F-12 medium in a 1:1 ratio (DMEM/F-12; Omega Scientific, cat. no. DM-25) B27 serum-free supplement (B27; Invitrogen/GIBCO, cat. no. 17504-044) Basic fibroblast growth factor-2 (FGF-2; PeproTech, cat. no. 100-18B-B) Epidermal growth factor (EGF; PeproTech, cat. no. 100-15) l-Glutamine (Invitrogen/GIBCO, cat. no. 2503-081) Antibiotic-antimycotic (Anti-Anti; Invitrogen/GIBCO, cat. no. 15240-062) as previously described in Guo et al. (2012).

Colonoid isolation and culture—Mouse colon organoids were generated from wild-type C57BL/6J and *Trp53*$^{-/-}$ mice. All mouse care and use were approved by the Institutional Animal Care and Use Committee at the Johns Hopkins University. *Trp53*$^{-/-}$ genotype was determined using the following primers: 5′-

CCCGAGTATCTGGAAGACAG-3′ and 5′-ATAGGTCGGCGGTTCAT-3′. Murine colon organoids were generated as previously described (Sato et al., 2011). The distal third of the colon was removed and rinsed with PBS. The distal colon was placed in complete chelating solution and minced. Minced tissue was then incubated with 150 rpm shaking in 31.25 mM EDTA in chelating solution for 30 minutes-1 hours at 4°C to release crypts. Tissue fragments were allowed to settle and supernatant containing crypts was collected. Crypts were centrifuged at 200 × g for 5 minutes and embedded in Matrigel and seeded on 24 well plates. After solidification of Matrigel, 500 μl WENR culture medium was added (Sato et al., 2011). Media was changed every 2 days and mCO were passaged using enzymatic dissociation with TrypLE Express every 7 days.

Generation of primary human mammary organoids—Normal mammary reduction samples were acquired from the Cooperative Human Tissue Network in compliance with a study protocol (NA_00077976) that was categorized as exempt/not human subject research by the Johns Hopkins School of Medicine Institutional Review Board. Each sample was deidentified prior to receipt and shipped overnight in basal DMEM/RPMI medium. Upon receipt, samples were washed with an anti-fungal solution, minced, and digested in a collagenase (Sigma C2139) solution. Normal mammary epithelial organoids were then enriched by performing a series of differential centrifugation steps, as previously described (Nguyen-Ngoc et al., 2012). Mammary organoids were then embedded in growth factor reduced Matrigel and cultured in the presence of medium containing EGF, hydrocortisone, insulin, and cholera toxin (Cheung et al., 2013).

METHOD DETAILS

Lentivirus production—Plasmids used: pMD2.G, psPAX2, pLV-H2B-Neon-ires-Puro. HEK293FT cells were co-transfected with the lentiviral transfer plasmid, packaging plasmid, and envelope plasmid. Media containing lentivirus was collected 24 and 48 hours after transfection. Lentivirus was concentrated using a centrifugal filter (Amicon Ultra-15, 100,000 NMWL). Lentiviral titer was determined by qPCR (abm qPCR Lentivirus Titration Kit, cat. # LV900).

Live imaging—mCO, HCT116 and RPE1 were transduced with H2B-Neon lentivirus as described previously (Bolhaqueiro et al., 2018, 2019). Following transduction, mCO were cultured in WENR culture media for 5–7 days. mCO were then dissociated to single cells and allowed to grow for 2 days in WENR culture media. Then, cells stably expressing the construct were selected with 1 μg/ml puromycin for 2–4 days. Transduced HCT116 and RPE1 cells were selected beginning 48 hours after addition of lentivirus using 1 μg/ml and 3 μg/ml puromycin, respectively. For live imaging, mCO, HCT116 and RPE1 were seeded on 8-well coverglass bottom chamber slides. 3–5 days after seeding for mCO and 2 days after seeding HCT116 and RPE1 cells were imaged using a laser-scanning confocal microscope (Zeiss 780). The environmental chamber was maintained at 37°C with 5% CO_2. Cells were imaged with a 40x water-immersion objective. Cells were imaged every 3–3.5 minutes with 15–20 2.0 μM z slices for mCO and 15–20 1.0 μM z slices for HCT116 and RPE1. Images were processed using a custom ImageJ macro modified from the ImageJ plugin “Temporal-Color Code” (Miura, 2010). Mitotic errors were scored manually.

Metaphase chromosome spreads—Chromosome spreads were obtained by arresting cells in mitosis in Karyomax Colcemid solution (1:100; Life Technologies) for 4–8 h, followed by harvesting using trypsin and/or accutase. Trypsinized cells were collected by centrifugation for 5 min at 300 × g and gently resuspended in a small amount of medium (~1 ml). Resuspended cells were allowed to swell for 7–10 min in 0.4% KCl solution at room temperature and prefixed by addition of freshly prepared methanol: acetic acid (3:1) fixative solution (~100 μL per 10 mL of total volume). Prefixed cells were collected by centrifugation and fixed in methanol:acetic acid (3:1) fixative solution. Spreads were dropped on a glass slide and incubated at 65°C for at least 1 h. For counting, spreads were mounted in Vectashield containing 4′,6-diamidino-2-phenylindole (DAPI; Vector Laboratories, Burlingame, CA), imaged on a Nikon TiE-Eclipse epifluorescence microscope (60 × oil immersion objective), and counted using the Cell Counter plug-in in ImageJ (Schneider et al., 2012)

Immunoblotting—Mammary organoids were isolated from Matrigel by incubation with dispase (Corning) at 37°C for 1 hr. Digestion was terminated by addition of 5 mM EDTA and organoids resuspended by trituration. Colon organoids were isolated from Matrigel by shaking at 150 rpm at 4°C in Cell Recovery Solution (Corning). Organoids and cells were pelleted at 200 g for 5 min and resuspended in RIPA buffer (50 mM Tris pH 8.0, 150 mM sodium chloride, 1% NP-40, 0.5% sodium deoxycholate, 0.1% SDS) containing Complete Mini Protease Inhibitor Cocktail (Roche). Lysates were homogenized by vortexing, incubated on ice for 20 min, and centrifuged at 13,000 rpm at 4°C for 20 min. Protein concentration of supernatants was measured using Bradford dye (Bio-Rad) on a spectrophotometer. Lysates were diluted in 5X sample buffer (250 mM Tris pH 6.8, 50% glycerol, 5% β-mercaptoethanol 0.025% bromophenol blue, 5% SDS). Samples were separated on homemade polyacrylamide gels or Bolt 4–12% Bis-Tris Plus gels (ThermoFisher) and transferred to Immobilon-P membranes (Millipore) via wet transfer or PVDF membranes via iBlot dry transfer (ThermoFisher). Membranes were blocked with 5% milk in TBST (50 mM Tris pH 8.0, 150 mM NaCl, 0.1% Tween-20) for 1 hr at room temperature. Membranes were incubated in primary antibodies diluted in 5% milk in TBST at 4°C with rocking for 16 hr and washed with TBST for 10 min thrice. Membranes were incubated in secondary antibodies diluted in TBST at room temperature with rocking for 1 hr and washed with TBST for 10 min thrice. Membranes were incubated in ECL Prime Western Blotting Detection Reagent (GE Healthcare) for 5 min and imaged on an ImageQuant LAS 4000 luminescent image analyzer (GE Healthcare).

Immunofluorescence—For p53 and pH2AX immunofluorescence, cells were fixed in 4% PFA/PBS for 15 min and permeabilized with 0.5% Triton X-100. Blocking was done with 5% boiled normal goat serum in PBS/0.5% Triton X-100. Primary and secondary antibodies were diluted in 2.5% (wt/vol) bovine serum albumin (BSA)/PBS/0.5% Triton X-100. Specimens were incubated with primary antibodies overnight, washed three times for 5–10 min, and incubated with fluorescently conjugated secondary antibodies for 2–4 h. All washes were performed with PBS/0.5% Triton X-100. DNA was counterstained with DAPI or Hoechst 33342 (Thermo Fisher Scientific). Vectashield (Vector Laboratories) was used for mounting. p53 and pH2AX images were acquired with the Nikon TiE-Eclipse

fluorescence microscope (20 × air and 60 × oil immersion objectives). For p53 immunofluorescence, three or four tiled images containing hundreds of cells were analyzed to determine the mean number of positive cells and the SD. At least 30 cells were imaged for each condition. Data were visualized and analyzed using ImageJ. After background subtraction, images were thresholded and the area of each object quantified using MetaMorph software. For pericentrin IF in mCO, cells were grown in 8 well glass-bottom coverslides and fixed with 4% paraformaldehyde for 10 min. Cells were permeabilized with for 1 hour at room temperature with 0.5% Triton X-100 in PBS and blocked for 3 hours at room temperature with 10% FBS + 0.1% Triton X-100 in PBS. Primary and secondary antibodies were diluted in 2% FBS + 0.1% Triton X-100. Specimens were incubated with primary antibodies overnight, washed three times for 10 minutes, and incubated with fluorescently conjugated secondary antibodies for 2 hours. All washes were performed with PBS. DNA was counterstained with DAPI and F-actin was labeled with Alexa Fluor 555 Phalloidin. Images were acquired using an LSM780 confocal microscope (40x water immersion objective). At least 8 organoids were imaged per condition.

EdU labeling—For EdU incorporation assays, cells were typically seeded in multiwell black, optically clear bottom, tissue culture–treated plates (PerkinElmer) for imaging and treated with 10 μM EdU (Thermo Fisher Scientific) for the indicated times. Cells were fixed in 4% paraformaldehyde (PFA)/phosphate-buffered saline (PBS) for 15 min and then permeabilized with 0.5% Triton X-100. Fixed cells were washed with PBS and stained with 1 μM Alexa Fluor 488 or Alexa Fluor 555–conjugated azide diluted in PBS containing 2 mM $CuSO_4$ and 50 mM ascorbic acid. To counterstain the DNA, Hoechst 33342 was added to 2 μg/ml. Cells were incubated for several hours or overnight at room temperature protected from light and evaporation and then washed three times with PBS. Later they were subjected to imaging using Nikon TiE-Eclipse epifluorescence microscope (60 × oil immersion objective) and/or Attune flow analyzer.

Image analysis—Nuclear and mitotic chromatin volumes in mCO were calculated using the commercial software Imaris, version 9.5. Nuclei and mitotic chromatin were segmented by H2B-mNeon (live imaging) or DAPI (fixed cells) fluorescence using the “Surface” function of Imaris. Volume of the generated surfaces was quantified and reported. Centrosomes were segmented using the “Spots” function of Imaris. Centrosome number per mitotic cell was manually counted following segmentation.

Doubling time analysis—Cell population doubling time was quantified in HCT116, RPE1, and *Trp53*$^{+/+}$ H2B-mNeon mCO. For the 2D cell lines (HCT116 and RPE1), cell number was counted using flow cytometry. Dead cells were identified and excluded from the cell count by staining with 1 μg/mL propidium iodide. To quantify mCO doubling time, *Trp53*$^{+/+}$ H2B-mNeon mCO were dissociated to single cells using TrypLE Express Enzyme (GIBCO, catalog 12604013) and plated in a 96 well glass-bottom imaging plate at a density of 3,000 cells per well. Twenty randomly selected mCO were imaged using a using a laser-scanning confocal microscope (Zeiss 780). Nuclei number per organoid was quantified by segmenting individual nuclei using the “Surface” function of Imaris as described above.

Doubling time was calculated by: $g = \frac{\ln\left(\frac{N(t)}{N(0)}\right)}{t}$. g = growth rate, N = average cell number, t = 24 hours. Doubling time $= \frac{\ln(2)}{g}$.

Drug Treatments—We used the following chemical inhibitors: MPS1 Inhibitor (NMS-P715) 0.4 μM for NPC and 1μM for all other cell lines and organoid cultures, Nutlin-3 at 1–5 μM, Bleomycin at 2.5 μg/ml, Doxorubicin at 0.5–5 μM, ZM 447439 at 1 μM, Nocodazole at 80nM and CalyculinA at 50 nM.

QUANTIFICATION AND STATISTICAL ANALYSIS

The number of biological replicates, the number of cells analyzed per biological replicate, and the statistical test performed are indicated in the figure legends. A biological replicate was defined as tissue or cells harvested from a single mouse or patient sample. Statistical tests performed and figures generated using Prism (GraphPad) and/or R-Studio. For all statistical tests, a cutoff of $p < 0.05$ was used to indicate significance.

Supplementary Material

Refer to Web version on PubMed Central for supplementary material.

ACKNOWLEDGMENTS

We thank Y. Wu for assistance in mouse NPC isolation and H. Zhang, J. Unruh, and T. Potapova for advice on experimental techniques. We thank the Hugo J.G. Snippert and Geert J.P.L. Kops labs at the University Medical Centre Utrecht for providing the pLV-H2B-Neon-ires-Puro plasmid and Andrew Holland's lab for providing *Trp53*$^{-/-}$ mice. B.A.J. received support from the NIH Medical Scientist Training Program T32GM136577. A.J.E. received support for this project through grants from The Breast Cancer Research Foundation (BCRF-19-048) and the NIH/NCI (U01CA217846, U54CA2101732, and 3P30CA006973). This work was supported by the grant R35 GM118172 from the National Institutes of Health and the ASPIRE Award from the Mark Foundation to R.L.

REFERENCES

Andreassen PR, Lohez OD, Lacroix FB, and Margolis RL (2001). Tetraploid state induces p53-dependent arrest of nontransformed mammalian cells in G1. Mol. Biol. Cell 12, 1315–1328. [PubMed: 11359924]

Artegiani B, Hendriks D, Beumer J, Kok R, Zheng X, Joore I, Chuva de Sousa Lopes S, van Zon J, Tans S, and Clevers H (2020). Fast and efficient generation of knock-in human organoids using homology-independent CRISPR-Cas9 precision genome editing. Nat. Cell Biol 22, 321–331. [PubMed: 32123335]

Aylon Y, and Oren M (2011). p53: guardian of ploidy. Mol. Oncol 5, 315–323. [PubMed: 21852209]

Beroukhim R, Mermel CH, Porter D, Wei G, Raychaudhuri S, Donovan J, Barretina J, Boehm JS, Dobson J, Urashima M, et al. (2010). The landscape of somatic copy-number alteration across human cancers. Nature 463, 899–905. [PubMed: 20164920]

Bolhaqueiro ACF, van Jaarsveld RH, Ponsioen B, Overmeer RM, Snippert HJ, and Kops GJPL (2018). Live imaging of cell division in 3D stem-cell organoid cultures. Methods Cell Biol. 145, 91–106. [PubMed: 29957217]

Bolhaqueiro ACF, Ponsioen B, Bakker B, Klaasen SJ, Kucukkose E, van Jaarsveld RH, Vivié J, Verlaan-Klink I, Hami N, Spierings DCJ, et al. (2019). Ongoing chromosomal instability and karyotype evolution in human colorectal cancer organoids. Nat. Genet 51, 824–834. [PubMed: 31036964]

Bunz F, Fauth C, Speicher MR, Dutriaux A, Sedivy JM, Kinzler KW, Vogelstein B, and Lengauer C (2002). Targeted inactivation of p53 in human cells does not result in aneuploidy. Cancer Res. 62, 1129–1133. [PubMed: 11861393]

Bykov VJN, Eriksson SE, Bianchi J, and Wiman KG (2018). Targeting mutant p53 for efficient cancer therapy. Nat. Rev. Cancer 18, 89–102. [PubMed: 29242642]

Cai Y, Crowther J, Pastor T, Abbasi Asbagh L, Baietti MF, De Troyer M, Vazquez I, Talebi A, Renzi F, Dehairs J, et al. (2016). Loss of Chromosome 8p Governs Tumor Progression and Drug Response by Altering Lipid Metabolism. Cancer Cell 29, 751–766. [PubMed: 27165746]

Chen G, Mulla WA, Kucharavy A, Tsai HJ, Rubinstein B, Conkright J, McCroskey S, Bradford WD, Weems L, Haug JS, et al. (2015). Targeting the adaptability of heterogeneous aneuploids. Cell 160, 771–784. [PubMed: 25679766]

Cheung KJ, Gabrielson E, Werb Z, and Ewald AJ (2013). Collective invasion in breast cancer requires a conserved basal epithelial program. Cell 155, 1639–1651. [PubMed: 24332913]

Cianchi F, Balzi M, Becciolini A, Giachè V, Messerini L, Palomba A, Tisti E, Faraoni P, Chellini F, Pucciani F, et al. (1999). Correlation between DNA content and p53 deletion in colorectal cancer. Eur. J. Surg 165, 363–368. [PubMed: 10365839]

Clausen OPF, Lothe RA, Børresen-Dale AL, De Angelis P, Chen Y, Rognum TO, and Meling GI (1998). Association of p53 accumulation with TP53 mutations, loss of heterozygosity at 17p13, and DNA ploidy status in 273 colorectal carcinomas. Diagn. Mol. Pathol 7, 215–223. [PubMed: 9917132]

Colombo R, Caldarelli M, Mennecozzi M, Giorgini ML, Sola F, Cappella P, Perrera C, Depaolini SR, Rusconi L, Cucchi U, et al. (2010). Targeting the mitotic checkpoint for cancer therapy with NMS-P715, an inhibitor of MPS1 kinase. Cancer Res. 70, 10255–10264. [PubMed: 21159646]

Crasta K, Ganem NJ, Dagher R, Lantermann AB, Ivanova EV, Pan Y, Nezi L, Protopopov A, Chowdhury D, and Pellman D (2012). DNA breaks and chromosome pulverization from errors in mitosis. Nature 482, 53–58. [PubMed: 22258507]

Darzynkiewicz Z, Halicka HD, Zhao H, and Podhorecka M (2011). Cell synchronization by inhibitors of DNA replication induces replication stress and DNA damage response: analysis by flow cytometry. Methods Mol. Biol 761, 85–96. [PubMed: 21755443]

Davoli T, Xu AW, Mengwasser KE, Sack LM, Yoon JC, Park PJ, and Elledge SJ (2013). Cumulative haploinsufficiency and triplosensitivity drive aneuploidy patterns and shape the cancer genome. Cell 155, 948–962. [PubMed: 24183448]

Dephoure N, Hwang S, O'Sullivan C, Dodgson SE, Gygi SP, Amon A, and Torres EM (2014). Quantitative proteomic analysis reveals posttranslational responses to aneuploidy in yeast. eLife 3, e03023. [PubMed: 25073701]

Donehower LA, Soussi T, Korkut A, Liu Y, Schultz A, Cardenas M, Li X, Babur O, Hsu TK, Lichtarge O, et al. (2019). Integrated Analysis of TP53 Gene and Pathway Alterations in The Cancer Genome Atlas. Cell Rep. 28, 1370–1384.e5. [PubMed: 31365877]

Drost J, van Jaarsveld RH, Ponsioen B, Zimberlin C, van Boxtel R, Buijs A, Sachs N, Overmeer RM, Offerhaus GJ, Begthel H, et al. (2015). Sequential cancer mutations in cultured human intestinal stem cells. Nature 521, 43–47. [PubMed: 25924068]

Duesberg P, Stindl R, and Hehlmann R (2001). Origin of multidrug resistance in cells with and without multidrug resistance genes: chromosome reassortments catalyzed by aneuploidy. Proc. Natl. Acad. Sci. USA 98, 11283–11288. [PubMed: 11553793]

Dulić V, Kaufmann WK, Wilson SJ, Tlsty TD, Lees E, Harper JW, Elledge SJ, and Reed SI (1994). p53-dependent inhibition of cyclin-dependent kinase activities in human fibroblasts during radiation-induced G1 arrest. Cell 76, 1013–1023. [PubMed: 8137420]

el-Deiry WS, Tokino T, Velculescu VE, Levy DB, Parsons R, Trent JM, Lin D, Mercer WE, Kinzler KW, and Vogelstein B (1993). WAF1, a potential mediator of p53 tumor suppression. Cell 75, 817–825. [PubMed: 8242752]

Foijer F, Xie SZ, Simon JE, Bakker PL, Conte N, Davis SH, Kregel E, Jonkers J, Bradley A, and Sorger PK (2014). Chromosome instability induced by Mps1 and p53 mutation generates aggressive lymphomas exhibiting aneuploidy-induced stress. Proc. Natl. Acad. Sci. USA 111, 13427–13432. [PubMed: 25197064]

Fujiwara T, Bandi M, Nitta M, Ivanova EV, Bronson RT, and Pellman D (2005). Cytokinesis failure generating tetraploids promotes tumorigenesis in p53-null cells. Nature 437, 1043–1047. [PubMed: 16222300]

Fukasawa K, Choi T, Kuriyama R, Rulong S, and Vande Woude GF (1996). Abnormal centrosome amplification in the absence of p53. Science 271, 1744–1747. [PubMed: 8596939]

Galipeau PC, Cowan DS, Sanchez CA, Barrett MT, Emond MJ, Levine DS, Rabinovitch PS, and Reid BJ (1996). 17p (p53) allelic losses, 4N (G2/tetraploid) populations, and progression to aneuploidy in Barrett's esophagus. Proc. Natl. Acad. Sci. USA 93, 7081–7084. [PubMed: 8692948]

Ganem NJ, and Pellman D (2007). Limiting the proliferation of polyploid cells. Cell 131, 437–440. [PubMed: 17981108]

Ganem NJ, Godinho SA, and Pellman D (2009). A mechanism linking extra centrosomes to chromosomal instability. Nature 460, 278–282. [PubMed: 19506557]

Gerstung M, Jolly C, Leshchiner I, Dentro SC, Gonzalez S, Rosebrock D, Mitchell TJ, Rubanova Y, Anur P, Yu K, et al.; PCAWG Evolution & Heterogeneity Working Group; PCAWG Consortium (2020). The evolutionary history of 2,658 cancers. Nature 578, 122–128. [PubMed: 32025013]

Giam M, Wong CK, Low JS, Sinelli M, Dreesen O, and Rancati G (2019). P53 Induces Senescence in the Unstable Progeny of Aneuploid Cells. bioRxiv. 10.1101/818112.

Graham NA, Minasyan A, Lomova A, Cass A, Balanis NG, Friedman M, Chan S, Zhao S, Delgado A, Go J, et al. (2017). Recurrent patterns of DNA copy number alterations in tumors reflect metabolic selection pressures. Mol. Syst. Biol 13, 914. [PubMed: 28202506]

Guo W, Patzlaff NE, Jobe EM, and Zhao X (2012). Isolation of multipotent neural stem or progenitor cells from both the dentate gyrus and subventricular zone of a single adult mouse. Nat. Protoc 7, 2005–2012. [PubMed: 23080272]

Hafner A, Bulyk ML, Jambhekar A, and Lahav G (2019). The multiple mechanisms that regulate p53 activity and cell fate. Nat. Rev. Mol. Cell Biol 20, 199–210. [PubMed: 30824861]

Halicka D, Zhao H, Li J, Garcia J, Podhorecka M, and Darzynkiewicz Z (2016). DNA damage response resulting from replication stress induced by synchronization of cells by inhibitors of DNA replication: Analysis by flow cytometry. Methods Mol. Biol 1524, 107–119.

Haupt Y, Maya R, Kazaz A, and Oren M (1997). Mdm2 promotes the rapid degradation of p53. Nature 387, 296–299. [PubMed: 9153395]

Hinchcliffe EH, Day CA, Karanjeet KB, Fadness S, Langfald A, Vaughan KT, and Dong Z (2016). Chromosome missegregation during anaphase triggers p53 cell cycle arrest through histone H3.3 Ser31 phosphorylation. Nat. Cell Biol 18, 668–675. [PubMed: 27136267]

Horii T, Yamamoto M, Morita S, Kimura M, Nagao Y, and Hatada I (2015). p53 suppresses tetraploid development in mice. Sci. Rep 5, 8907. [PubMed: 25752699]

Hurwitz R, Hozier J, LeBien T, Minowada J, Gajl-Peczalska K, Kubonishi I, and Kersey J (1979). Characterization of a leukemic cell line of the pre-B phenotype. Int. J. Cancer 23, 174–180. [PubMed: 83966]

Janssen A, van der Burg M, Szuhai K, Kops GJPL, and Medema RH (2011). Chromosome segregation errors as a cause of DNA damage and structural chromosome aberrations. Science 333, 1895–1898. [PubMed: 21960636]

Kastenhuber ER, and Lowe SW (2017). Putting p53 in Context. Cell 170, 1062–1078. [PubMed: 28886379]

Kaya A, Gerashchenko MV, Seim I, Labarre J, Toledano MB, and Gladyshev VN (2015). Adaptive aneuploidy protects against thiol peroxidase deficiency by increasing respiration via key mitochondrial proteins. Proc. Natl. Acad. Sci. USA 112, 10685–10690. [PubMed: 26261310]

Knouse KA, Lopez KE, Bachofner M, and Amon A (2018). Chromosome Segregation Fidelity in Epithelia Requires Tissue Architecture. Cell 175, 200–211.e13. [PubMed: 30146160]

Kollu S, Abou-Khalil R, Shen C, and Brack AS (2015). The Spindle Assembly Checkpoint Safeguards Genomic Integrity of Skeletal Muscle Satellite Cells. Stem Cell Reports 4, 1061–1074. [PubMed: 25960061]

Kruse JP, and Gu W (2009). Modes of p53 regulation. Cell 137, 609–622. [PubMed: 19450511]

Kurinna S, Stratton SA, Coban Z, Schumacher JM, Grompe M, Duncan AW, and Barton MC (2013). p53 regulates a mitotic transcription program and determines ploidy in normal mouse liver. Hepatology 57, 2004–2013. [PubMed: 23300120]

Lambrus BG, Daggubati V, Uetake Y, Scott PM, Clutario KM, Sluder G, and Holland AJ (2016). A USP28-53BP1-p53-p21 signaling axis arrests growth after centrosome loss or prolonged mitosis. J. Cell Biol 214, 143–153. [PubMed: 27432896]

Lane AA, Chapuy B, Lin CY, Tivey T, Li H, Townsend EC, van Bodegom D, Day TA, Wu SC, Liu H, et al. (2014). Triplication of a 21q22 region contributes to B cell transformation through HMGN1 overexpression and loss of histone H3 Lys27 trimethylation. Nat. Genet 46, 618–623. [PubMed: 24747640]

Lee AJX, Endesfelder D, Rowan AJ, Walther A, Birkbak NJ, Futreal PA, Downward J, Szallasi Z, Tomlinson IPM, Howell M, et al. (2011). Chromosomal instability confers intrinsic multidrug resistance. Cancer Res. 71, 1858–1870. [PubMed: 21363922]

Lengauer C, Kinzler KW, and Vogelstein B (1998). Genetic instabilities in human cancers. Nature 396, 643–649. [PubMed: 9872311]

Lens SMA, and Medema RH (2019). Cytokinesis defects and cancer. Nat. Rev. Cancer 19, 32–45. [PubMed: 30523339]

Li M, Fang X, Baker DJ, Guo L, Gao X, Wei Z, Han S, van Deursen JM, and Zhang P (2010). The ATM-p53 pathway suppresses aneuploidy-induced tumorigenesis. Proc. Natl. Acad. Sci. USA 107, 14188–14193. [PubMed: 20663956]

Lopes CAM, Mesquita M, Cunha AI, Cardoso J, Carapeta S, Laranjeira C, Pinto AE, Pereira-Leal JB, Dias-Pereira A, Bettencourt-Dias M, and Chaves P (2018). Centrosome amplification arises before neoplasia and increases upon p53 loss in tumorigenesis. J. Cell Biol 217, 2353–2363. [PubMed: 29739803]

López-García C, Sansregret L, Domingo E, McGranahan N, Hobor S, Birkbak NJ, Horswell S, Grönroos E, Favero F, Rowan AJ, et al. (2017). BCL9L Dysfunction Impairs Caspase-2 Expression Permitting Aneuploidy Tolerance in Colorectal Cancer. Cancer Cell 31, 79–93. [PubMed: 28073006]

McKinley KL, and Cheeseman IM (2017). Large-Scale Analysis of CRISPR/Cas9 Cell-Cycle Knockouts Reveals the Diversity of p53-Dependent Responses to Cell-Cycle Defects. Dev. Cell 40, 405–420.e2. [PubMed: 28216383]

Mello SS, and Attardi LD (2018). Deciphering p53 signaling in tumor suppression. Curr. Opin. Cell Biol 51, 65–72. [PubMed: 29195118]

Mijit M, Caracciolo V, Melillo A, Amicarelli F, and Giordano A (2020). Role of p53 in the Regulation of Cellular Senescence. Biomolecules 10, 420.

Mirkovic M, Guilgur LG, Tavares A, Passagem-Santos D, and Oliveira RA (2019). Induced aneuploidy in neural stem cells triggers a delayed stress response and impairs adult life span in flies. PLoS Biol. 17, e3000016. [PubMed: 30794535]

Miura K (2010). Temporal-Color Code (version 101123).

Muller PAJ, and Vousden KH (2013). p53 mutations in cancer. Nat. Cell Biol 15, 2–8. [PubMed: 23263379]

Navin N, Kendall J, Troge J, Andrews P, Rodgers L, McIndoo J, Cook K, Stepansky A, Levy D, Esposito D, et al. (2011). Tumour evolution inferred by single-cell sequencing. Nature 472, 90–94. [PubMed: 21399628]

Nguyen-Ngoc KV, Cheung KJ, Brenot A, Shamir ER, Gray RS, Hines WC, Yaswen P, Werb Z, and Ewald AJ (2012). ECM microenvironment regulates collective migration and local dissemination in normal and malignant mammary epithelium. Proc. Natl. Acad. Sci. USA 109, E2595–E2604. [PubMed: 22923691]

Nowell PC (1976). The clonal evolution of tumor cell populations. Science 194, 23–28. [PubMed: 959840]

Olivier M, Hollstein M, and Hainaut P (2010). TP53 mutations in human cancers: origins, consequences, and clinical use. Cold Spring Harb. Perspect. Biol 2, a001008. [PubMed: 20182602]

Oren M (1999). Regulation of the p53 tumor suppressor protein. J. Biol. Chem 274, 36031–36034. [PubMed: 10593882]

Pavelka N, Rancati G, Zhu J, Bradford WD, Saraf A, Florens L, Sanderson BW, Hattem GL, and Li R (2010). Aneuploidy confers quantitative proteome changes and phenotypic variation in budding yeast. Nature 468, 321–325. [PubMed: 20962780]

Potapova TA, Seidel CW, Box AC, Rancati G, and Li R (2016). Transcriptome analysis of tetraploid cells identifies cyclin D2 as a facilitator of adaptation to genome doubling in the presence of p53. Mol. Biol. Cell 27, 3065–3084. [PubMed: 27559130]

Prokocimer M, Molchadsky A, and Rotter V (2017). Dysfunctional diversity of p53 proteins in adult acute myeloid leukemia: projections on diagnostic workup and therapy. Blood 130, 699–712. [PubMed: 28607134]

R Core Team (2019). R: A language and environment for statistical computing (R Foundation for Statistical Computing).

Rehen SK, Yung YC, McCreight MP, Kaushal D, Yang AH, Almeida BSV, Kingsbury MA, Cabral KMS, McConnell MJ, Anliker B, et al. (2005). Constitutional aneuploidy in the normal human brain. J. Neurosci 25, 2176–2180. [PubMed: 15745943]

Reinhardt HC, and Schumacher B (2014). The p53 network : Cellular and systemic DNA damage responses in aging and cancer. Trends Genet. 28, 128–136.

Robles AI, Jen J, and Harris CC (2016). Clinical outcomes of TP53 mutations in cancers. Cold Spring Harb. Perspect. Med 6, a026294. [PubMed: 27449973]

RStudio Team (2020). RStudio: Integrated Development for R (R Foundation for Statistical Computing).

Sack LM, Davoli T, Li MZ, Li Y, Xu Q, Naxerova K, Wooten EC, Bernardi RJ, Martin TD, Chen T, et al. (2018). Profound Tissue Specificity in Proliferation Control Underlies Cancer Drivers and Aneuploidy Patterns. Cell 173, 499–514.e23. [PubMed: 29576454]

Salic A, and Mitchison TJ (2008). A chemical method for fast and sensitive detection of DNA synthesis in vivo. Proceedings of the National Academy of Sciences 105, 2415–2420.

Santaguida S, Richardson A, Iyer DR, M'Saad O, Zasadil L, Knouse KA, Wong YL, Rhind N, Desai A, and Amon A (2017). Chromosome Mis-segregation Generates Cell-Cycle-Arrested Cells with Complex Karyotypes that Are Eliminated by the Immune System. Dev. Cell 41, 638–651.e5. [PubMed: 28633018]

Sato T, and Clevers H (2013). Primary mouse small intestinal epithelial cell cultures. Methods Mol. Biol 945, 319–328. [PubMed: 23097115]

Sato T, Stange DE, Ferrante M, Vries RGJ, Van Es JH, Van den Brink S, Van Houdt WJ, Pronk A, Van Gorp J, Siersema PD, and Clevers H (2011). Long-term expansion of epithelial organoids from human colon, adenoma, adenocarcinoma, and Barrett's epithelium. Gastroenterology 141, 1762–1772. [PubMed: 21889923]

Schneider CA, Rasband WS, and Eliceiri KW (2012). NIH Image to ImageJ: 25 years of image analysis. Nat. Methods 9, 671–675. [PubMed: 22930834]

Schutgens F, and Clevers H (2020). Human Organoids: Tools for Understanding Biology and Treating Diseases. Annu. Rev. Pathol 15, 211–234. [PubMed: 31550983]

Selmecki A, Forche A, and Berman J (2006). Aneuploidy and isochromosome formation in drug-resistant Candida albicans. Science 313, 367–370. [PubMed: 16857942]

Shen H, and Maki CG (2011). Pharmacologic activation of p53 by small-molecule MDM2 antagonists. Curr. Pharm. Des 17, 560–568. [PubMed: 21391906]

Shi Q, and King RW (2005). Chromosome nondisjunction yields tetraploid rather than aneuploid cells in human cell lines. Nature 437, 1038–1042. [PubMed: 16222248]

Simões-Sousa S, Littler S, Thompson SL, Minshall P, Whalley H, Bakker B, Belkot K, Moralli D, Bronder D, Tighe A, et al. (2018). The p38α Stress Kinase Suppresses Aneuploidy Tolerance by Inhibiting Hif-1α. Cell Rep. 25, 749–760.e6. [PubMed: 30332653]

Soto M, Raaijmakers JA, Bakker B, Spierings DCJ, Lansdorp PM, Foijer F, and Medema RH (2017). p53 Prohibits Propagation of Chromosome Segregation Errors that Produce Structural Aneuploidies. Cell Rep. 19, 2423–2431. [PubMed: 28636931]

Steigemann P, Wurzenberger C, Schmitz MHA, Held M, Guizetti J, Maar S, and Gerlich DW (2009). Aurora B-mediated abscission checkpoint protects against tetraploidization. Cell 136, 473–484. [PubMed: 19203582]

Sterkers Y, Lachaud L, Bourgeois N, Crobu L, Bastien P, and Pagès M (2012). Novel insights into genome plasticity in Eukaryotes: mosaic aneuploidy in Leishmania. Mol. Microbiol 86, 15–23. [PubMed: 22857263]

Stichel D, Ebrahimi A, Reuss D, Schrimpf D, Ono T, Shirahata M, Reifenberger G, Weller M, Hänggi D, Wick W, et al. (2018). Distribution of EGFR amplification, combined chromosome 7 gain and chromosome 10 loss, and TERT promoter mutation in brain tumors and their potential for the reclassification of IDHwt astrocytoma to glioblastoma. Acta Neuropathol. 136, 793–803. [PubMed: 30187121]

Sulak M, Fong L, Mika K, Chigurupati S, Yon L, Mongan NP, Emes RD, and Lynch VJ (2016). *TP53* copy number expansion is associated with the evolution of increased body size and an enhanced DNA damage response in elephants. eLife 5, e11994. [PubMed: 27642012]

Sunshine AB, Payen C, Ong GT, Liachko I, Tan KM, and Dunham MJ (2015). The fitness consequences of aneuploidy are driven by condition-dependent gene effects. PLoS Biol. 13, e1002155. [PubMed: 26011532]

Taylor AM, Shih J, Ha G, Gao GF, Zhang X, Berger AC, Schumacher SE, Wang C, Hu H, Liu J, et al.; Cancer Genome Atlas Research Network (2018). Genomic and Functional Approaches to Understanding Cancer Aneuploidy. Cancer Cell 33, 676–689.e3. [PubMed: 29622463]

Terradas M, Martín M, Tusell L, and Genescà A (2009). DNA lesions sequestered in micronuclei induce a local defective-damage response. DNA Repair (Amst.) 8, 1225–1234. [PubMed: 19683478]

Thompson SL, and Compton DA (2010). Proliferation of aneuploid human cells is limited by a p53-dependent mechanism. J. Cell Biol 188, 369–381. [PubMed: 20123995]

Torres EM, Sokolsky T, Tucker CM, Chan LY, Boselli M, Dunham MJ, and Amon A (2007). Effects of aneuploidy on cellular physiology and cell division in haploid yeast. Science 317, 916–924. [PubMed: 17702937]

Uetake Y, and Sluder G (2004). Cell cycle progression after cleavage failure: mammalian somatic cells do not possess a “tetraploidy checkpoint”. J. Cell Biol 165, 609–615. [PubMed: 15184397]

Wasylishen AR, and Lozano G (2016). Attenuating the p53 pathway in human cancers: Many means to the same end. Cold Spring Harb. Perspect. Med 6, a026211. [PubMed: 27329033]

Watson EV, and Elledge SJ (2017). Aneuploidy Police Detect Chromosomal Imbalance Triggering Immune Crackdown!. Trends Genet. 33, 662–664. [PubMed: 28800914]

Weaver BA, and Cleveland DW (2006). Does aneuploidy cause cancer? Curr. Opin. Cell Biol 18, 658–667. [PubMed: 17046232]

Wickham H (2016). ggplot2: Elegant Graphics for Data Analysis (Springer-Verlag New York).

Wong C, and Stearns T (2005). Mammalian cells lack checkpoints for tetraploidy, aberrant centrosome number, and cytokinesis failure. BMC Cell Biol. 6, 6. [PubMed: 15713235]

Yang AH, Kaushal D, Rehen SK, Kriedt K, Kingsbury MA, McConnell MJ, and Chun J (2003). Chromosome segregation defects contribute to aneuploidy in normal neural progenitor cells. J. Neurosci 23, 10454–10462. [PubMed: 14614104]

Yang F, Teoh F, Tan ASM, Cao Y, Pavelka N, and Berman J (2019). Aneuploidy Enables Cross-Adaptation to Unrelated Drugs. Mol. Biol. Evol 36, 1768–1782. [PubMed: 31028698]

Yona AH, Manor YS, Herbst RH, Romano GH, Mitchell A, Kupiec M, Pilpel Y, and Dahan O (2012). Chromosomal duplication is a transient evolutionary solution to stress. Proc. Natl. Acad. Sci. USA 109, 21010–21015. [PubMed: 23197825]

Zack TI, Schumacher SE, Carter SL, Cherniack AD, Saksena G, Tabak B, Lawrence MS, Zhsng CZ, Wala J, Mermel CH, et al. (2013). Pan-cancer patterns of somatic copy number alteration. Nat. Genet 45, 1134–1140. [PubMed: 24071852]

Zhang CZ, Spektor A, Cornils H, Francis JM, Jackson EK, Liu S, Meyerson M, and Pellman D (2015). Chromothripsis from DNA damage in micronuclei. Nature 522, 179–184. [PubMed: 26017310]

Highlights

- Cell lines exhibit variable p53 dependence in growth arrest after aneuploidy
- Aneuploidy induction does not activate p53 or arrest growth in organotypic cultures
- p53 knockout increases mitotic errors and aneuploidy production in colon organoids

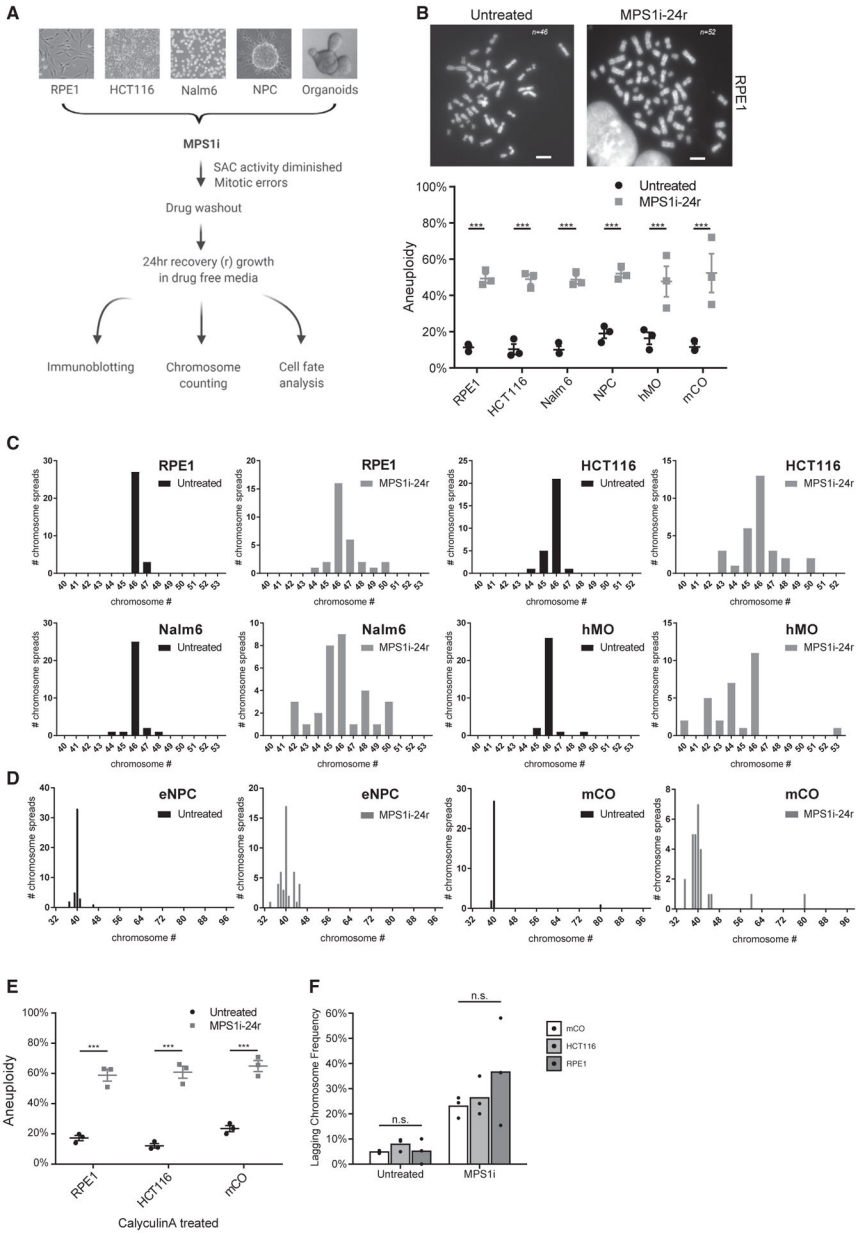

Figure 1. Induction of aneuploidy with MPS1i in mammalian cell lines and 3D organotypic cultures

(A) Schematic of the workflow to induce aneuploidy and detect p53 regulation in RPE1, HCT116, Nalm6, neural progenitor cells (NPCs), and organoids and downstream cell fate analysis.

(B) Representative images of metaphase spreads from untreated and MPS1i-treated RPE1 cells (top). Quantification of the percent of metaphase spreads with an aneuploid chromosome number in each cellular model (bottom). Cell lines RPE1, HCT116, Nalm6, human mammary organoid (hMO), and mouse colon organoid (mCO) were treated with 1 μM MPS1i and 400 nM for mouse NPCs for 24 h, followed by drug washout and recovery growth in drug-free media for 24 h before sample collection. n ≥ 3 biological replicates; n ≥ 30 mitoses counted for each condition per replicate. Scale bar, 10 μm.

(C and D) Histograms represent the number of spreads with the indicated number of chromosomes by metaphase spreads of cell lines and organoid cultures as described in (B).
(E) Percent aneuploidy for calyculin-A-treated RPE1, HCT116, and mCOs. n ≥ 30 mitotic spreads counted for each condition.
(F) Lagging chromosome frequency quantified by live-cell imaging of H2B-mNeon-labeled cells. MPS1i was added 1 h prior to the start of imaging. n = 3 biological replicates, n > 120 mitoses scored per condition for mCO and HCT116, and n > 40 mitoses scored per condition for RPE1.
Error bars represent mean ± SEM. *p ≤ % 0.05; **p ≤ % 0.01; ***p ≤ % 0.001; one-tailed Fisher's exact test (B, D, and E) and one-way ANOVA (F); n.s., not significant.

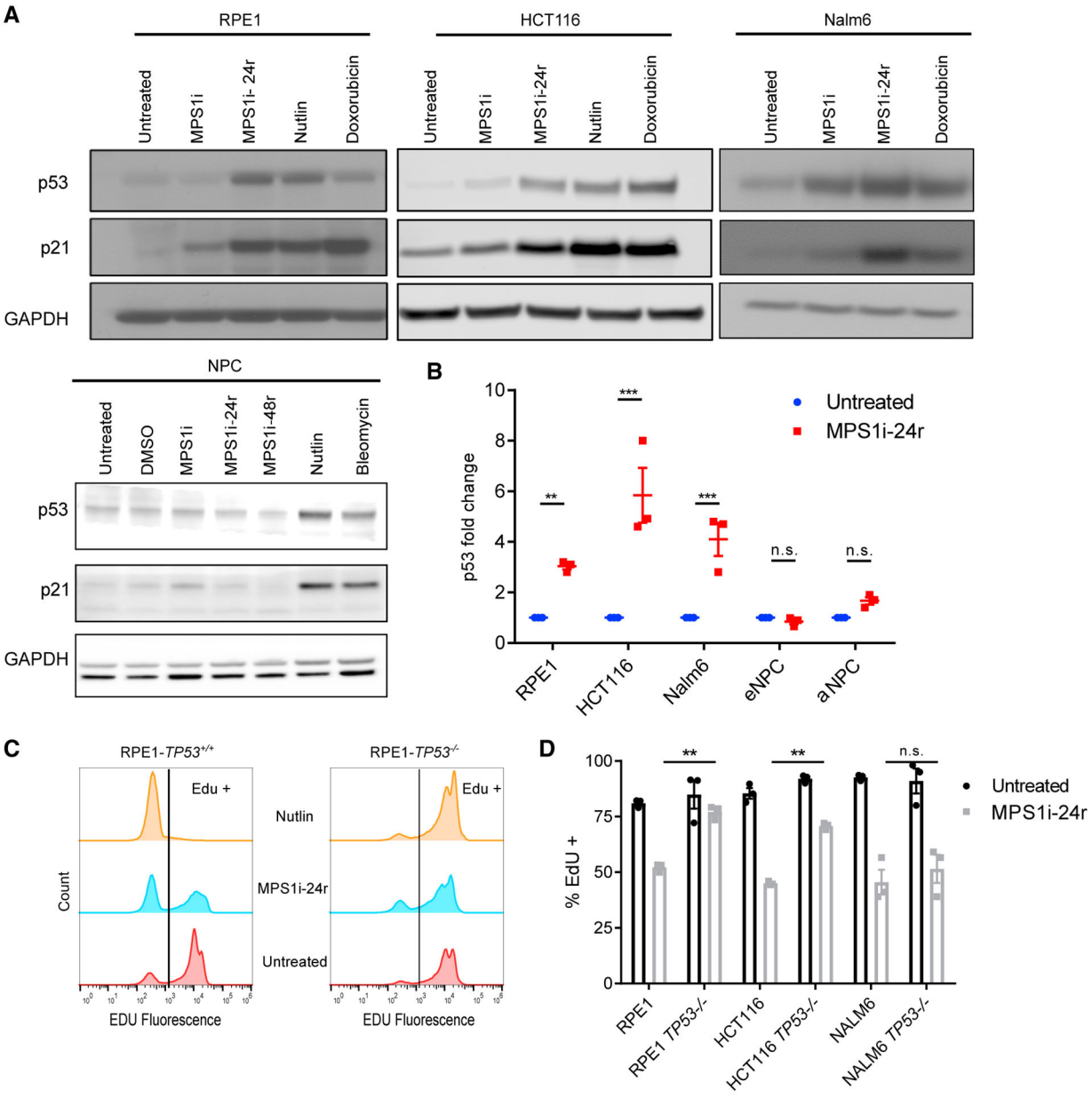

Figure 2. Adherent RPE1 and HCT116 but not suspension Nalm6 cells depend on p53 for growth arrest after aneuploidy induction

(A) Levels of p53 and p21 as determined by immunoblot analysis. Unsynchronized populations of mammalian cell lines RPE1, HCT116, and Nalm6 and NPCs either untreated or MPS1i treated for 24 h followed by drug washout and recovery growth in drug-free media for 24 h or 48 h. Bleomycin, doxorubicin, and nutlin were used as positive controls for p53 and p21 induction. GAPDH served as a loading control.

(B) Quantification of p53 fold change by densitometry analysis; n ≥ 3 biological replicates of the data in (A).

(C) Representative fluorescence-activated cell sorting (FACS) profiles of EdU incorporation in untreated, MPS1i-treated with drug-free recovery, and nutlintreated *TP53*$^{+/+}$ or *TP53*$^{-/-}$ RPE1 cells.

(D) Quantification of the percentages of EdU+ cells from the FACS data; n ≥ 3 biological replicates in the same experiment as in (C). Graphs show mean ± SEM. *p ≤ % 0.05, **p ≤ % 0.01, ***p ≤ % 0.001; multiple t test (B) and one-tailed Fisher's exact test (D); n.s., not significant.

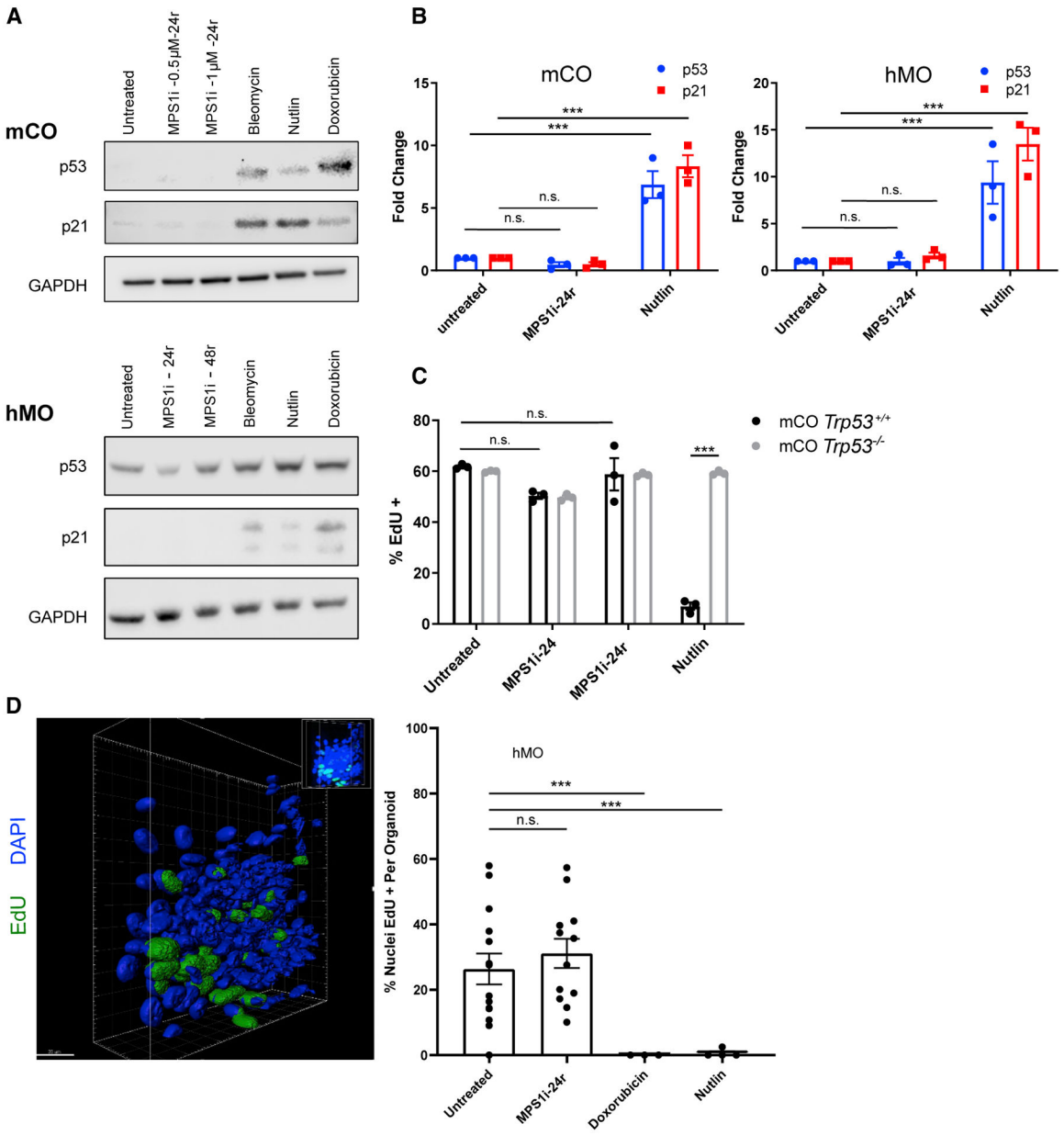

Figure 3. 3D organotypic cultures do not activate p53 or undergo growth arrest in response to aneuploidy

(A) Representative immunoblots from mCOs and hMOs showing p53 and p21 protein abundance after aneuploidy induction with MPS1i and positive-control cells treated with bleomycin, nutlin, or doxorubicin.

(B) Quantification of p53 and p21 fold change by densitometry analysis; n ≥ 3 biological repeats of the data in (A).

(C) Quantification of the percentages of EdU+ cells from the FACS data; n ≥ 3 biological replicates in *Trp53*$^{+/+}$ and *Trp53*$^{-/-}$ mCOs either untreated or treated with MPS1i, followed by EdU incorporation for 16 h.

(D) 3D reconstruction of a hMOs showing EdU+ cells along with quantification; n ≥ 3 biological replicates. Scale bar, 20 μm.

Graphs show mean ± SEM. *p ≤ % 0.05, **p ≤ % 0.01, ***p ≤ % 0.001; multiple t test (B) and one-tailed Fisher's exact test (D); n.s., not significant.

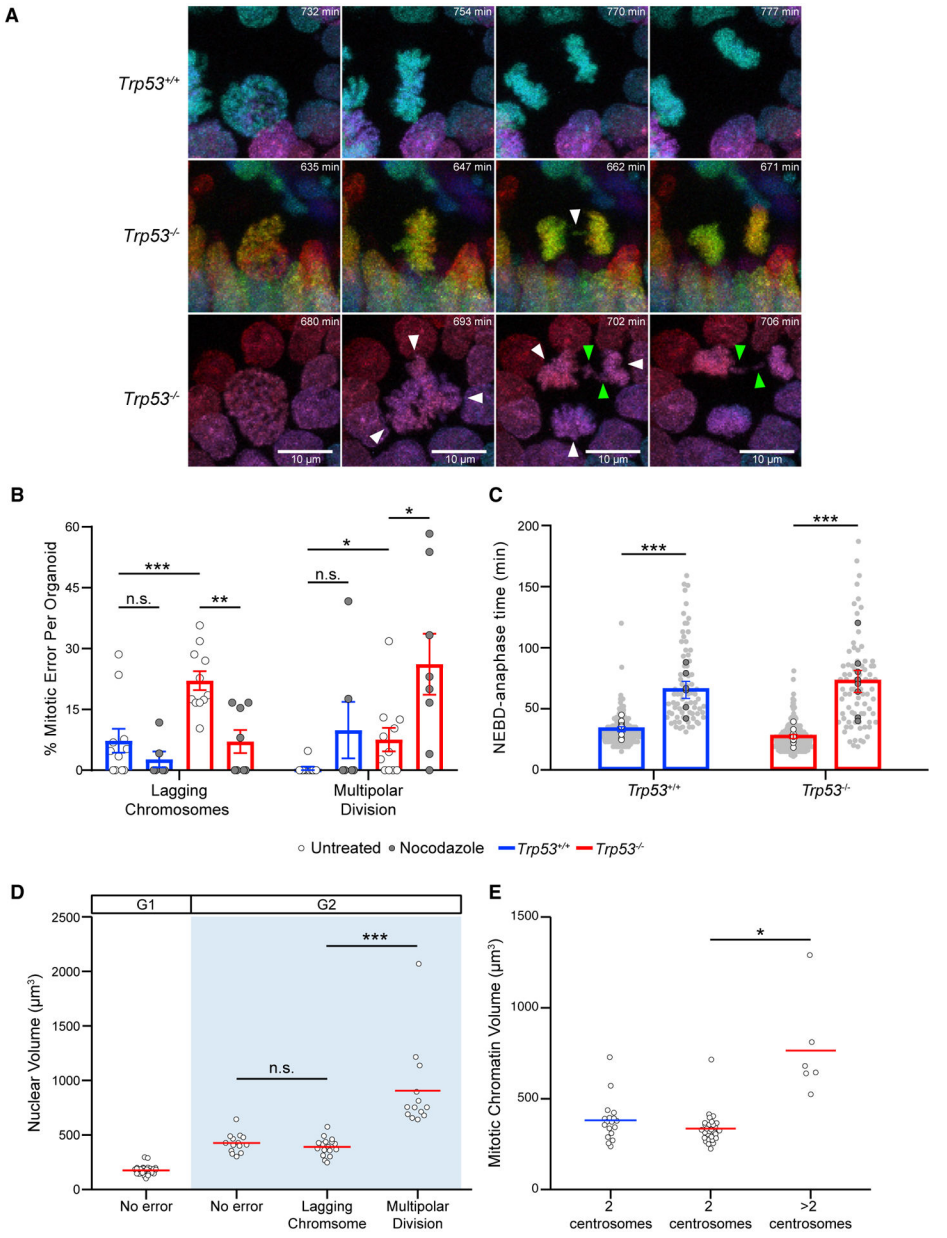

Figure 4. *Trp53*$^{-/-}$ mCOs exhibit frequent mitotic aberrations

(A) Representative frames from time-lapse videos of *Trp53*$^{+/+}$ and *Trp53*$^{-/-}$ mCOs with chromosomes labeled with H2B-mNeon undergoing normal mitosis (top row), mitosis with lagging chromosomes (middle row), and multipolar mitosis (bottom row). Arrowheads indicate relevant mitotic aberrations. Scale bars, 10 μm.

(B) Quantification of the percentage of mitoses with a mitotic error in untreated and 80 nM nocodazole-treated *Trp53*$^{+/+}$ and *Trp53*$^{-/-}$ mCOs. Each data point represents one organoid. Percentage was obtained by dividing the number of mitoses with an error by the total number of mitoses observed. n ≥ 6 organoids observed per condition, n > 150 divisions scored for untreated *Trp53*$^{+/+}$ and *Trp53*$^{-/-}$, and n > 80 divisions scored for nocodazole-treated *Trp53*$^{+/+}$ and *Trp53*$^{-/-}$.

(C) Quantification of time from nuclear envelope breakdown (NEBD) to anaphase onset. Points with black outlines represent the mean of one organoid. Light-gray points represent one mitosis. n > 150 divisions scored for untreated *Trp53*$^{+/+}$ and *Trp53*$^{-/-}$, and n > 80 divisions scored for nocodazole-treated *Trp53*$^{+/+}$ and *Trp53*$^{-/-}$.

(D) Quantification of nuclear volume immediately prior to (G2) or after (G1) mitosis in H2B-mNeon *Trp53*$^{-/-}$ mCO.s Each point represents one nucleus. n ≥ 6 organoids observed per replicate.

(E) Quantification of mitotic chromatin volume and centrosome number of dividing cells in *Trp53*$^{+/+}$ and *Trp53*$^{-/-}$ mCOs. Chromatin was labeled using DAPI, and centrosome number was quantified by pericentrin immunofluorescence (IF) staining. n ≥ 8 organoids per replicate.

Bars in (B) and (C) represent mean ± SEM of n ≥ 6 total organoids for n = 3 independent experiments. Lines in (D) and (E) represent mean of all data points. *p ≤ % 0.05, **p ≤ % 0.01, ***p ≤ % 0.001; Wilcoxon rank-sum test (B and C) or unpaired Welch's unequal variances t test (D and E). See also Videos S1, S2, S3, and S4.

KEY RESOURCES TABLE

REAGENT or RESOURCE	SOURCE	IDENTIFIER
Antibodies		
Anti-p53 [DO-1], mouse monoclonal	Abcam	Cat# ab1101; RRID:AB_297667
Anti-p53 (1C12), mouse monoclonal	Cell Signaling	Cat# 2524; RRID:AB_331743
Anti-p21 Waf1/Cip1 (12D1), rabbit monoclonal	Cell Signaling	Cat# 2947; RRID:AB_823586
Anti-p21 Waf1/Cip1 (F-5), mouse monoclonal	Santa Cruz	Cat# sc-6246; RRID:AB_628073
Anti-GAPDH (D16H11), rabbit monoclonal	Cell Signaling	Cat# 5174; RRID:AB_10622025
Anti-pericentrin, mouse monoclonal	BD Biosciences	Cat# 611814; RRID:AB_399294
Anti-phospho-histone H2A.X (Ser-139), rabbit monoclonal	Cell Signaling	Cat #9718; RRID:AB_2118009
Anti-rabbit IgG, HRP-linked Antibody	Cell Signaling	Cat# 7074; RRID:AB_2099233
Anti-mouse IgG, HRP-linked Antibody	Cell Signaling	Cat# 7076; RRID:AB_330924
Alexa Fluor 488 Polyclonal Antibody	ThermoFisher	Cat# A-11094; RRID:AB_221544
Biological samples		
Normal human mammary reduction samples	Cooperative Human Tissue Network	https://www.chtn.org/
Chemicals, peptides, and recombinant proteins		
NMS-P715	EMD/Millipore	Cat# 475949
Nutlin-3	Sigma Aldrich	Cat# N6287
Bleomycin	EMD/Millipore	Cat# 203410
Nocodazole	Sigma Aldrich	Cat# M1404
ZM 447439	Selleckchem	Cat# S1103
Calyculin A	Cayman Chemical	Cat# 19246
Doxorubicin	Sigma Aldrich	Cat# AMBH324A4B72
Critical commercial assays		
Click-iT EdU Alexa Fluor 488	Invitrogen	Cat# C10420
Annexin V, Alexa Fluor 488 conjugate	Invitrogen	Cat# A13201
Experimental models: cell lines		
RPE-1 hTERT	ATCC	CRL-4000
RPE-1 *TP53*$^{-/-}$	Laboratory of Andrew Holland	N/A
HCT116	Laboratory of Bert Vogelstein	N/A
HCT116 *TP53*$^{-/-}$	Laboratory of Bert Vogelstein	N/A
Nalm6	Laboratory of Mike Tyers	N/A
Nalm6 *TP53*$^{-/-}$	This study	N/A
Experimental models: organisms/strains		
Mouse: wild-type C57BL/6J	The Jackson Laboratory	RRID:IMSR_JAX:000664
Mouse: B6.129S2-Trp53^{tm1Tyj}/J	The Jackson Laboratory	RRID:IMSR_JAX:002101
Recombinant DNA		
pLV-H2B-Neon-ires-Puro	Bolhaqueiro et al., 2018, 2019	N/A
pMD2.G	Laboratory of Didier Trono	RRID:Addgene_12259
psPAX2	Laboratory of Didier Trono	RRID:Addgene_12260
Software and algorithms		

REAGENT or RESOURCE	SOURCE	IDENTIFIER
ImageJ	Schneider et al., 2012	https://imagej.nih.gov/ij/
IMARIS	Oxford Instruments 2021	https://imaris.oxinst.com/
Prism (version 8)	Graphpad	N/A
R, version 3.6.1	R Core Team, 2019	https://www.R-project.org/
RStudio, version 1.1.463	RStudio Team, 2020	https://www.rstudio.com/
ggplot2, version 3.2.1	Wickham, 2016	https://ggplot2.tidyverse.org/